



Intracellular delivery of proteins for live cell imaging

Ban-Seok Jeong^a, Hwanhee C. Kim^b, Catherine M. Sniezek^{c,1}, Stephanie Berger^{c,1}, Justin M. Kollman^{d,*}, David Baker^{c,d,e,**}, Joshua C. Vaughan^{b,f,***}, Xiaohu Gao^{a,*}

^a Department of Bioengineering, University of Washington, United States of America

^b Department of Chemistry, University of Washington, United States of America

^c Institute for Protein Design, University of Washington, United States of America

^d Department of Biochemistry, University of Washington, United States of America

^e Howard Hughes Medical Institute, University of Washington, United States of America

^f Department of Neurobiology and Biophysics, University of Washington, United States of America

ARTICLE INFO

Keywords:

Cytosolic delivery
Small molecule
Protein
Antibody
Live-cell imaging
Drug discovery

ABSTRACT

The majority of cellular functions are regulated by intracellular proteins, and regulating their interactions can unlock fundamental insights in biology and open new avenues for drug discovery. Because the vast majority of intracellular targets remain undruggable, there is significant current interest in developing protein-based agents especially monoclonal antibodies due to their specificity, availability, and established screening/engineering methods. However, efficient delivery of proteins into the cytoplasm has been a major challenge in biological engineering and drug discovery. We previously reported a platform technology based on a Coomassie blue-cholesterol conjugate (CB-tag) capable of delivering small proteins directly into the cytoplasm. Here, we report a new generation of CB-tag that can bring proteins with a wide size range into the cytoplasm, bypassing endosomal sequestration. Remarkably, intracellular targets with distinct structures were visualized. Overall, the new CB-tag demonstrated a robust ability in protein delivery with broad applications ranging from live-cell immunofluorescence to protein-based therapeutic development.

1. Introduction

Intracellular delivery of functional proteins to live cells holds tremendous potential for the development of therapeutics and diagnostics, such as understanding protein-protein interactions, replacing defective enzymes, modulating signaling pathways, and promoting targeted protein degradation [1]. Because of the large binding interfaces, proteins can interact with a wide range of biological targets, many of which have been considered “undruggable” by traditional small-molecule drugs. This unique advantage enables them to distinguish subtle differences in targets, such as post-translational modifications, point mutations, quaternary structures, and splice variants with high specificity and affinity [2–5]. Hence, various protein-based affinity reagents such as antibodies, antibody fragments, nanobodies, affibodies, monobodies, DARPin, and *de novo*-designed minibinders have been developed for imaging and therapeutic applications [6–13].

Among them, antibodies play a prominent role because of the broad availability of *in vitro* and *in vivo* validated antibodies [14]. However, their use has been largely limited to the extracellular space including membrane receptors and secreted antigens due to the impermeability of proteins through the membrane of live cells [15]. This limitation has resulted in intracellular therapeutic targets, which comprise approximately 70 % of all proteins encoded by the human genome [16], underexplored.

To expand the scope of antibodies to treat intracellular targets and perform live-cell immunofluorescence imaging, efficient and robust cytosolic protein delivery is crucial. In this context, a wide range of delivery technologies have been developed based on cell-penetrating peptides [17–20], inorganic nanomaterials [21,22], polymers [23–33], and lipids [34–36], but the delivery efficiency is often hampered by the endocytic cell entry pathway where protein cargos are degraded inside endosomes and lysosomes [37–40]. To tackle this bottleneck, recent

* Corresponding author.

** Corresponding author at: Institute for Protein Design, University of Washington, United States of America.

*** Corresponding author at: Department of Chemistry, and Department of Neurobiology and Biophysics, University of Washington, United States of America
E-mail addresses: jkoll@uw.edu (J.M. Kollman), dabaker@uw.edu (D. Baker), jcv2@uw.edu (J.C. Vaughan), xgao@uw.edu (X. Gao).

¹ Current address: CMS: Department of Genome Sciences, University of Washington, Seattle, WA 98195; SB: 5870 Road H, Hebron, NE 68370

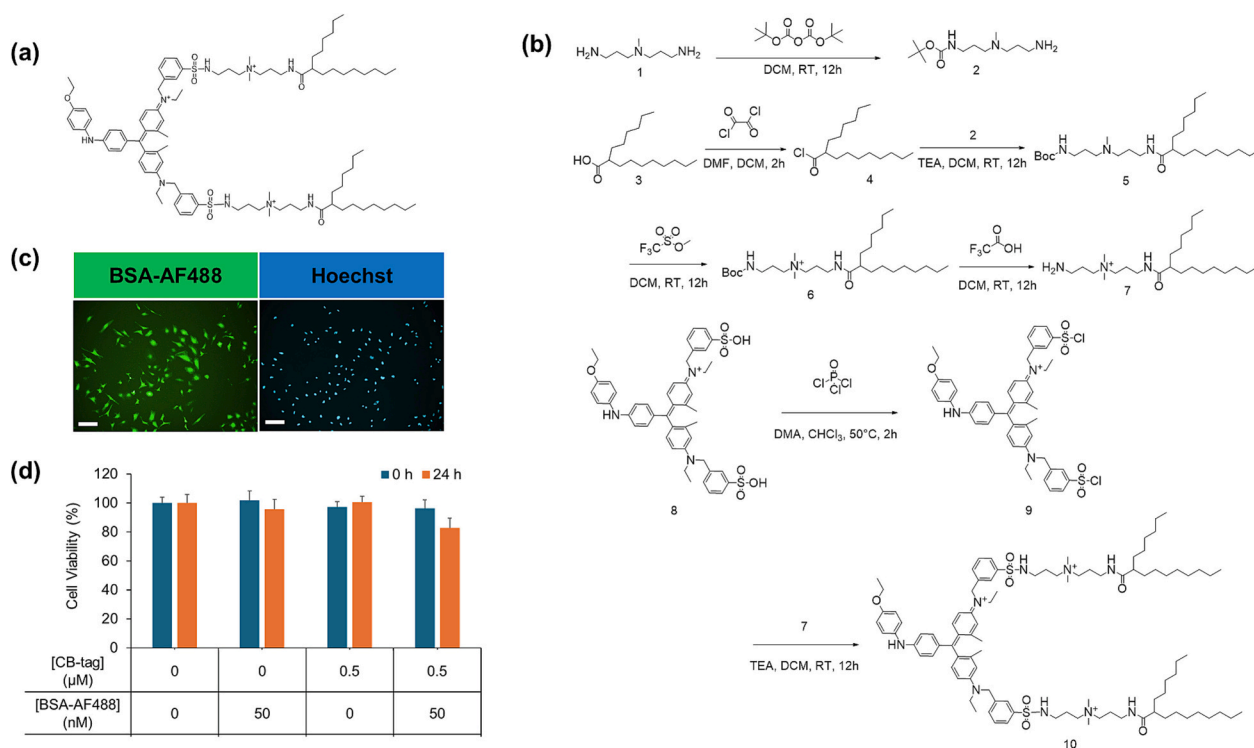


Fig. 1. Synthesis and characterization of the new CB-tag. (a) Chemical structure of the CB-Tag. (b) CB-tag synthetic route. Hexyl decanoyl chloride (4) was reacted with the linker 2 to obtain compound 5, whose tertiary amine is subsequently methylated to the quaternary amine (6). After t-Boc deprotection, two copies of 7 were conjugated to CB, resulting in the final product 10. (c) Representative images of HeLa cells after intracellular delivery of BSA-AF488 (BSA concentration 50 nM, Tag ratio 1:10). Scale bar denotes 100 μm . (d) Cell viability evaluation by the Alamar Blue assay of tag-BSA-AF488 complex in HeLa cells immediately after protein delivery (0 h) or after further incubation of 24 h (24 h). ([BSA-AF488] = 50 nM, Protein:Tag = 1:10) Results are presented as mean \pm standard deviation (S.D.) ($n = 4$). (For interpretation of the references to color in this figure legend, the reader is referred to the web version of this article.)

strategies focused on direct translocation of proteins across the plasma membrane to avoid the difficulties of endosomal escape and to deliver proteins into hard-to-transfect cells that have low endocytic activities. Several methods rely on transient membrane disruption using physical techniques such as microinjection, electroporation, sonoporation, photoporation, and microfluidics [41–43]. These methods bring down the membrane barrier between the extracellular and intracellular spaces for cargo protein entry but require high concentrations of the cargo protein and often result in cell injury and reduced viability [44]. Alternatively, chemical approaches based on the complexes of protein and cationic gold nanoparticles [45–48], polymers [49–51], phase separating peptides [52–55], or lipids [56] have also been developed to translocate proteins directly into the cytosol. These complexes can quickly enter the cytosol after getting in contact with the cell membrane [57,58].

In this context, our group recently developed a unique biologic cytosolic delivery technology by non-covalently tagging proteins with cholesterol [59]. The non-covalent association was achieved by modifying cholesterol molecules with CB, a protein-binding dye. When mixed with protein molecules, the CB end binds to proteins while the cholesterol end faces outward. Biomolecules non-covalently tagged by cholesterol were believed to enter cells through an initial membrane fusion followed by biomolecule-tag dissociation. The hydrophobic tag molecules are largely confined in the hydrophobic lipid bilayer while the hydrophilic biomolecule can quickly slip into the cytosol, bypassing the endocytosis. Although the exact mechanism of cell entry is not entirely clear, remarkable delivery efficiency has been observed for both small RNAs and proteins. A key limitation, however, is the protein size. While small proteins such as aprotinin (6.5 kDa) and lysozyme (15 kDa) showed high cytosolic delivery efficiency manifested by bright, diffuse, cytosolic fluorescence, large proteins such as BSA (66 kDa) and IgG (150 kDa) exhibited large puncta with low-level diffuse fluorescence,

indicating significant endosome entrapment. As a result, although the concept of CB-tag is appealing, its application scope is limited to small protein binders whose current availability is no match to that of full-size antibodies. Here, we report the design of the second-generation CB-tag in which the bulky cholesterol was replaced by branched alkyl chains (Fig. 1a). This new and structurally simpler tag can deliver large proteins including antibodies into the cytosol at high efficiency, substantially expanding the application of CB-tags.

2. Materials & methods

2.1. Materials and instruments

Triethylamine (TEA), Diisopropylethylamine (DIPEA), Triton X-100 (TX-100), Cytochalasin D, Methyl- β -cyclodextrin, Chlorpromazine hydrochloride, 5-(N-ethyl-N-isopropyl)amiloride, Sodium azide, Aprotinin, Bovine serum albumin (BSA), Lysozyme, Cytochrome-C (Cyt-C), Transferrin, Myoglobin, β -Lactoglobulin, Horseradish Peroxidase, Ovalbumin, and Avidin were purchased from Sigma-Aldrich (St. Louis and Burlington, MA). Alexa fluor 488, 555, 568 – NHS esters, Protein G-AF488, Streptavidin-AF555, Goat anti-Rabbit 2 $^{\circ}$ IgG-AF555, Vimentin monoclonal antibody (V9), Vimentin monoclonal antibody (V9)-AF488, Vimentin monoclonal antibody (V9)-AF555, Beta-actin monoclonal antibody (15G5A11/E2)-AF555, Alpha tubulin monoclonal antibody (TU-01)-AF555, Beta tubulin monoclonal antibody (BT7R)-AF555, SM (PEG)₂, SM(PEG)₁₂, NHS-PEG₁₂-Biotin, Hoechst 33342, and Mito-Tracker Green FM were purchased from ThermoFisher (Waltham, MA). Phalloidin-lysine was purchased from AAT Bioquest (Pleasanton, CA). 7-O-(Amino-PEG₄)-paclitaxel was purchased from BroadPharm (San Diego, CA). Phosphate-buffered saline (PBS), Dulbecco's Modified Eagle's Medium (DMEM), Opti-MEM, fetal bovine serum (FBS), and

penicillin/streptomycin were obtained from Gibco (Waltham, MA). CellTiter-Blue cell viability assay kit was purchased from Promega. μ -Slide 4-well glass bottom chambered coverslips were purchased from Ibidi (Fitchburg, WI). NMR spectra were obtained on Bruker AVANCE I 300 MHz and AVANCE III 500 MHz spectrometers and the chemical shifts are reported in parts per million (ppm). Electron spray ionization (ESI)-mass spectra (MS) were measured on a Bruker EsquireLC ion trap mass spectrometer

2.2. Protein fluorescence labeling

Proteins were dissolved in pH 9.5 Borate buffer saline (10 mM) at 5 mg/ml, and fluorescent dye (AF488, AF555, or AF568) stock solution in DMSO (10 mg/ml) was added into the protein solution and quickly mixed by pipetting. The molar ratio of dye to protein was typically 10:1. The reaction mixture was placed on a rocker for overnight incubation in the dark at room temperature. The excessive unconjugated dyes were removed by desalting spin columns while the buffer was exchanged for phosphate buffer (pH 7.4, 10 mM Phosphate, 0 mM NaCl). The obtained protein solution was diluted to 10 - 50 μ M and stored at 4 °C in the dark. The degree of labeling of Alexa Fluor 488, 555, or 568 to proteins was calculated from UV-Vis absorption spectra of the labeled proteins, according to the manufacturer's protocol. For antibodies supplied with stabilizing proteins such as BSA, protein A/G spin column (Thermo Scientific) was used following the manufacturer's protocol. For proteins pre-labeled with fluorescent dyes, a simple buffer exchange to phosphate buffer (10 mM phosphate, 0 mM NaCl) was performed first.

2.3. Conjugating paclitaxel or phalloidin to aprotinin-AF555

Aprotinin-AF555 (40 μ M) was treated with 5 mM TCEP in PBS for 30 min at RT, followed by purification to remove unreacted TCEP and buffer exchange to phosphate buffer (10 mM phosphate, 0 mM NaCl) using desalting spin columns. Paclitaxel- or Phalloidin-maleimide conjugates (1 mM in DMSO) at a molar ratio of 4:1 (PTX or Phalloidin conjugate:Aprotinin) was added to the protein solution and quickly mixed by pipetting. The mixture was stirred for 60 min at RT in the dark.

2.4. Cell culture

HeLa (human cervical carcinoma) and COS-7 (African green monkey kidney fibroblast cells) were cultured in DMEM supplemented with 10 % FBS and 1 % penicillin and streptomycin at 37 °C and 5 % CO₂.

2.5. Protein tagging by the CB-tag

CB-tag was dissolved in ethanol/water (4:1, v/v) to a concentration of 1.6 mM and stored at -20 °C as a stock. The concentration of the protein solutions was adjusted between 1 and 40 μ M (depending on the available concentration of commercially obtained proteins) in 5 mM phosphate buffer containing 0.015 % (w/v) TX-100. The CB-tag solution was added to the protein solution and quickly mixed by pipetting. Typically, the mixture was incubated for 30 min at RT, followed by further dilution with Opti-MEM to a final protein concentration of 50 nM before adding to cells. For (strept)avidin and IgG, incubation times of 5 min and 15 min, respectively, were sufficient.

2.6. Intracellular protein delivery

Cells were seeded into 24-well plates at a seeding density of 5.0×10^4 cells per well one day before the experiments. For confocal microscopy, cells were seeded onto μ -Slide 4 well glass coverslips at a seeding density of 6.3×10^4 cells per well. The experiments were conducted at about 80 % confluency to avoid cell senescence. The cell culture medium was gently aspirated, and the cell monolayer was washed once with pre-warmed Opti-MEM. After the removal of Opti-MEM, the tagged

protein was added to cells (e.g., 400 μ l per well for 24-well plates) and incubated for 2 h. Subsequently, the cells were washed with Opti-MEM, counterstained with Hoechst 33342 (100 ng/ml, 30 min), and imaged immediately.

2.7. Cell viability

Cell viability was determined using Alamar Blue either immediately after or 24 h post protein delivery. 80 μ l of CellTiter-Blue reagent (Promega) was added and the culture was incubated for 1 h before being assessed on a microplate reader (Tecan) at excitation/emission wavelengths of 560/590 nm. Viability was calculated according to the manufacturer's protocol.

2.8. Endocytosis inhibition assay

HeLa cells were pretreated with DMEM containing cytochalasin D (CytD, 10 μ M), 5-(N-ethyl-N-isopropyl)amiloride (EIPA, 50 μ M), Methyl- β -cyclodextrin (M β CD, 10 mM), chlorpromazine (CPZ, 15 μ M), or sodium azide (NaN₃, 100 mM) for 1 h in a cell incubator. Untreated cells were used as control. The cells were washed once with Opti-MEM, and the media were replaced by Opti-MEM containing tagged Aprotinin-AF555. After 2-h incubation, cells were washed once with Opti-MEM and counterstained with Hoechst 33342, and observed immediately by fluorescence microscopy. To study the effect of low temperature (4 °C), HeLa cells were incubated at 4 °C for 30 min before protein delivery. The cells were washed once with cold media (Opti-MEM) and treated with a cold solution of tagged protein in Opti-MEM. The cells were incubated at 4 °C for 3 h before washing with cold media and imaging.

2.9. Microscopy

For confocal microscopy, a Zeiss LSM 710 confocal laser-scanning microscope fitted with a plan apochromat objective (100 \times or 60 \times) was used. Alexa Fluor 488 was excited with a 488 nm argon ion laser, and fluorescence was recorded through a frame scan. Hoechst 33342 was excited with a 405 nm diode laser. Alexa Fluor 555 and 568 were excited by a 561 nm HeNe laser. For epi-fluorescence microscopy, an Olympus IX-71 inverted microscope was used with 40 \times and 10 \times objectives.

2.10. Live cell time-lapse imaging

Time-lapse images were captured every 30 s on an inverted Nikon Eclipse Ti2 fluorescence microscope equipped with a stage-top incubator (humidified with 5 % CO₂ at 37 °C). Before protein delivery, cells were preincubated with Hoechst 33342 (100 ng/ml, 30 min) and MitoTracker Green FM (100 nM, 30 min). Cells were washed once with pre-warmed Opti-MEM, added with tagged proteins in 400 μ l Opti-MEM, and immediately moved into the stage-top incubator and imaged.

3. Results and discussions

3.1. Synthesis of the new CB-tag and optimization of delivery conditions

The synthetic route is illustrated in Fig. 1b. Briefly, the sulfonic acid groups of CB G-250 were activated with phosphorus(V) oxychloride for conjugation with compound 7. Detailed chemical characterizations such as mass spectrometry and ¹H NMR of the intermediates and final product confirmed the molecular structures and purity of the new tag (Supplementary Figs. S1–8). The molecular weight and the isotopic pattern of the tag match the expected values, proving successful synthesis of the second-generation CB-tag (Supplementary Fig. S8).

Using the new tag, we first optimized the protein intracellular delivery conditions using bovine serum albumin (BSA) as a model cargo because of its availability and the challenge of efficient delivery with the

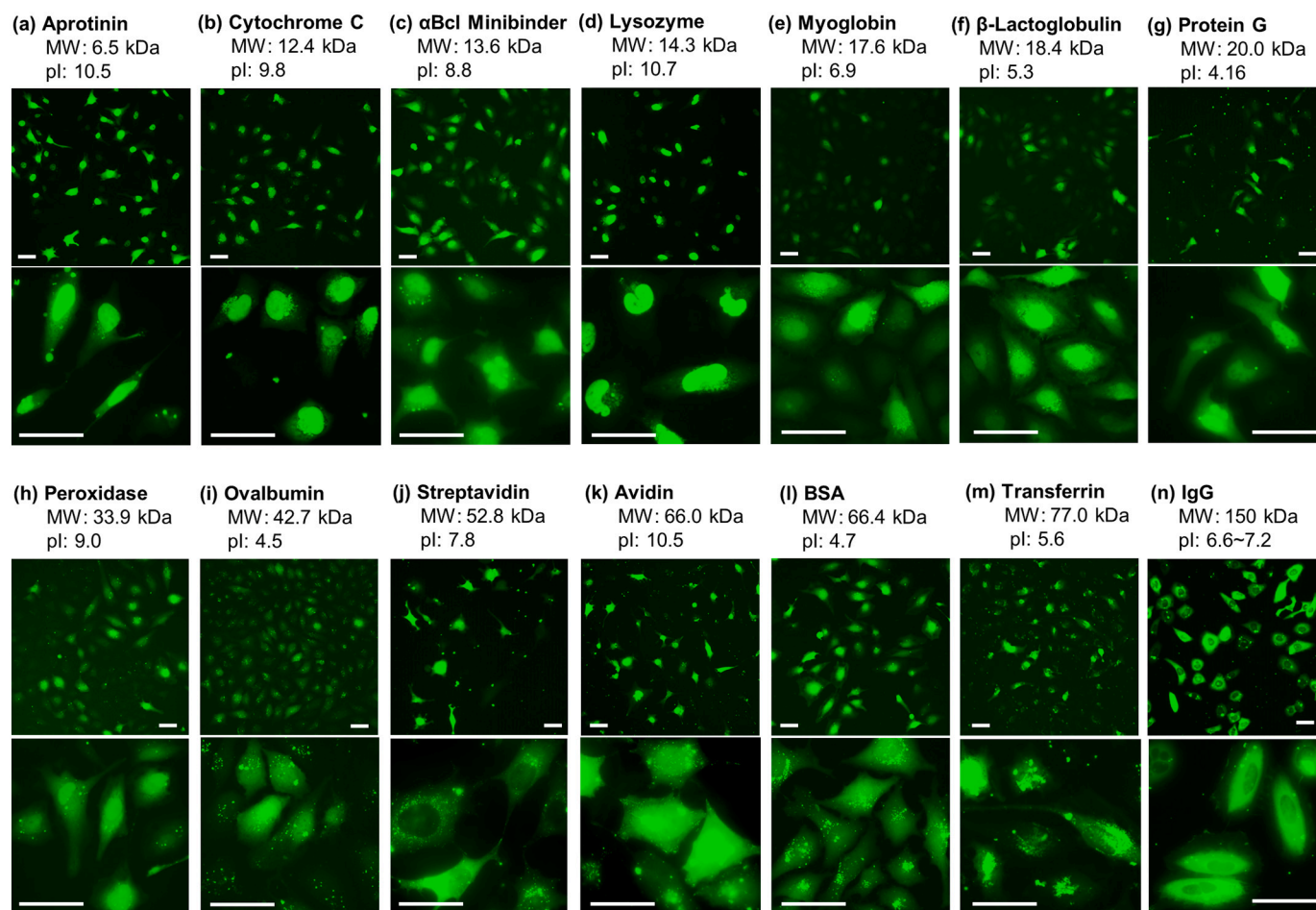


Fig. 2. HeLa cells after intracellular delivery of various proteins imaged at low-magnification (10 \times) to show the cell population with proteins successfully delivered and at high-magnification (40 \times) to show the protein intracellular distribution. (a) Aprotinin-AF555, 50 nM, Tag ratio = 1:2. (b) Cytochrome C-AF555, 100 nM, Tag ratio = 1:22. (c) α BCL Minibinder-AF488, 100 nM, Tag ratio = 1:2. (d) Lysozyme-AF555, 100 nM, Tag ratio = 1:10. (e) Myoglobin-AF568, 100 nM, Tag ratio = 1:8. (f) β -Lactoglobulin-AF568, 100 nM, Tag ratio 1:12. (g) Protein G-AF488, 100 nM, Tag ratio 1:6. (h) Horseradish Peroxidase-AF568, 100 nM, Tag ratio 1:1. (i) Ovalbumin-AF568, 100 nM, Tag ratio 1:16. (j) Streptavidin-AF555, 100 nM, Tag ratio 1:6. (k) Avidin-AF555, 100 nM, Tag ratio = 1:2. (l) BSA-AF488, 50 nM, Tag ratio 1:10. (m) Transferrin-AF555, 100 nM, Tag ratio = 1:6. (n) Secondary IgG-AF555, 100 nM, Tag ratio 1:10. Scale bar denotes 40 μ m.

first-generation CB-tag. The BSA molecules were labeled with Alexa Fluor 488 (AF488) with 4 dyes per protein molecule as estimated by UV-Vis absorption. This degree of labeling can be adjusted depending on protein size (higher for larger proteins). In an optimized buffer that contains a trace amount of TX-100 (0.015 %) that helps reduce protein aggregation during tagging and improve delivery efficiency, the fluorescently labeled BSA and CB-tag (molar ratio: 1:10) were incubated for 30 min before being diluted in Opti-MEM (final concentrations BSA 50 nM, and CB-tag 500 nM) and added to cells for intracellular delivery (2-h incubation). Note that although the final concentration of TX-100 was very low ($1.5 \times 10^{-4}\%$) and non-toxic to cells, it was highly effective in preventing the tagged proteins from aggregation. It has been well documented that TX-100 becomes toxic to cells when its concentration reaches the critical micelle concentration (CMC) in the range of 0.2 mM [60] ($\sim 100\times$ higher than the conditions used here). Remarkably, the new CB-tag not only brought fluorescent BSA molecules inside the cytosol at high efficiency (>90 % cells showing bright and homogeneous fluorescence without significant punctate fluorescent clusters, Fig. 1c), but also achieved it at a BSA concentration of 50 nM, 20-fold lower than previously used conditions (1 μ M) [59]. This optimized condition can substantially improve the affordability of protein-based imaging and drug discovery studies, and reduce potential toxicity caused by the CB-tag. Quantitative cell viability studies showed that at a CB-tag concentration of 500 nM, the toxicity was negligible with or without the BSA

cargo (50 nM) (Fig. 1d).

3.2. Intracellular delivery of proteins of various sizes

After optimizing the protocol of cytosolic delivery using BSA, proteins with a wide range of molecular weight (M.W., 6.5–150.0 kDa) and net charge (pI 4.2–10.7) were tested. In our previous report, only small proteins such as aprotinin (M.W. 6.5 kDa) and lysozyme (M.W. 15 kDa) could be efficiently transported into the cytosol. Larger proteins had a greater fraction of proteins trapped in endosomes over delivered cytosolically. In the current work, by changing cholesterol in the original CB-tag to branched alkyl chains, remarkably, large proteins such as BSA (M.W. 66.4 kDa), and full IgG (secondary IgG, M.W. 150 kDa) exhibited strong diffuse fluorescence indicating efficient delivery to the cell cytosol (Fig. 2). Among the 15 proteins tested, it was also interesting to observe that small proteins especially the ones with high PI values (positively charged at neutral pH) also had strong nucleus localization, possibly due to the high negative charges of nucleic acids. This protein nuclear localization also proved that the delivered proteins were not trapped inside endosomes [61].

3.3. Confirmation of non-endocytic cell entry

To further confirm the new CB-tag brings proteins inside cells via a

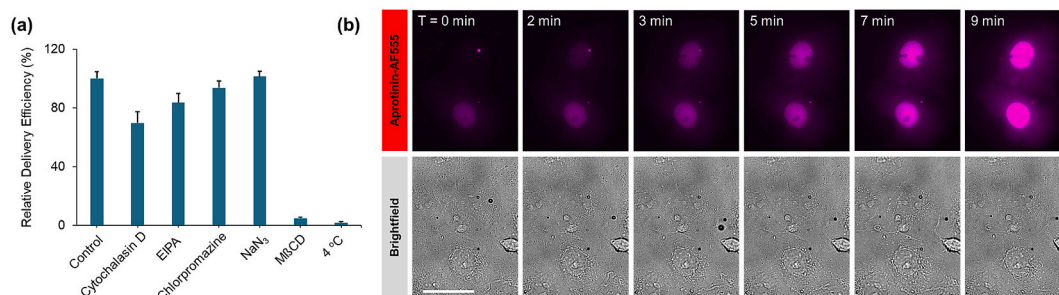


Fig. 3. Confirmation of protein cell entry *via* non-endocytic pathway. (a) Relative percentage of HeLa cells exhibiting diffuse fluorescence in cytosol pretreated with various inhibitors for 1 h, followed by incubating with the complex of Aprotinin-AF555 and CB-tag for 2 h in cell incubator. [Aprotinin-AF555] = 50 nM, Protein:Tag = 1:2. (b) Time-lapse imaging of HeLa cells during delivery of Aprotinin-AF555. (100 nM, Tag ratio = 1:2, Supplementary Fig. S13 and Video S1) Scale bar denotes 20 μ m.

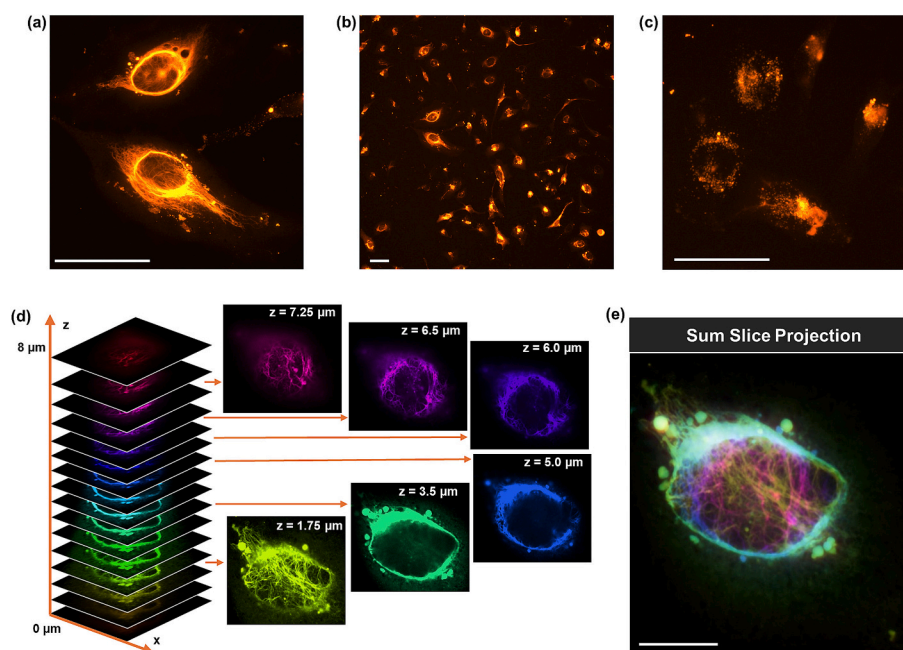


Fig. 4. Representative images of HeLa cells after intracellular delivery of anti-Vimentin IgG-AF568. ([IgG-AF568] = 50 nM, Tag ratio 1:10) with objective (a) 40 \times or (b) 10 \times , or (c) after overnight incubation. Scale bar denotes 40 μ m. (d) Representative confocal Z-stack images of HeLa cells after intracellular delivery of anti-Vimentin IgG-AF568. ([IgG-AF568] = 50 nM, Tag ratio 1:10) Z-stack slices were depth color-coded, and (e) Sum slices projection was applied to all z-stack slices by ImageJ. (3D projection in Supplementary Video 2) Scale bar denotes 10 μ m.

non-endocytic pathway, we investigated the cellular entry mechanism by pretreating cells with common endocytosis inhibitors including cytochalasin D (actin microfilament depolymerizer), 5-(N-ethyl-N-isopropyl)amiloride (EIPA, pinocytosis inhibitor), chlorpromazine hydrochloride (clathrin-mediated endocytosis inhibitor), sodium azide (NaN₃, energy-dependent endocytosis inhibitor), and methyl- β -cyclodextrin (M β CD, cholesterol depleting agent) before cytosolic delivery of aprotinin-AF555. As shown in Fig. 3a, only M β CD abolished protein internalization (similar to low-temperature treatment at 4 °C) while endocytosis and pinocytosis inhibitors showed minor reductions, confirming that the protein cell entry largely avoided the classic endocytic pathway.

The non-endocytic pathway was further confirmed by time-lapse imaging (Fig. 3b, Supplementary Fig. S13, and Video S1). A gradual increase of diffuse fluorescence in the cytosol and nucleus was observed, as opposed to the initial appearance of punctate spots from endocytosis and subsequent release from endosomes, which is similar to other studies reporting direct cytosolic delivery [45,48,50,55,56]. The time it takes for protein entry into the cell cytoplasm is highly heterogeneous, likely due to the heterogeneity of cells as well as the cell cycles they are

in. Because Coomassie blue alone is not highly fluorescent, dissociation between the noncovalently bound CB-tag and protein was not observed. However, due to the hydrophobicity of the tag, the CB tag is likely left in the cell membrane as the protein slipped inside the cells. Indeed, previously using siRNA and an RNA-tag composed of an RNA binding dye and a cholesterol, siRNA-tag dissociation was observed [62].

3.4. Cytosolic delivery of primary antibodies

Next, we proceeded with the delivery of primary antibodies and testing of their functionality in recognizing intracellular targets. We chose three cytoskeleton targets, vimentin intermediate filament, actin microfilament, and microtubule, because of their distinctive filamentous structures from which specific or non-specific binding can be easily discerned. Anti-vimentin monoclonal antibody (V9) was selected to label intermediate filaments. As shown in Fig. 4a, when anti-vimentin IgG-AF568 was delivered into HeLa cells, filaments were observed in the cells, indicating that the antibodies were functional and remained correctly folded during delivery. Low-magnification fluorescence imaging also confirmed the delivery efficiency (most of the cells are

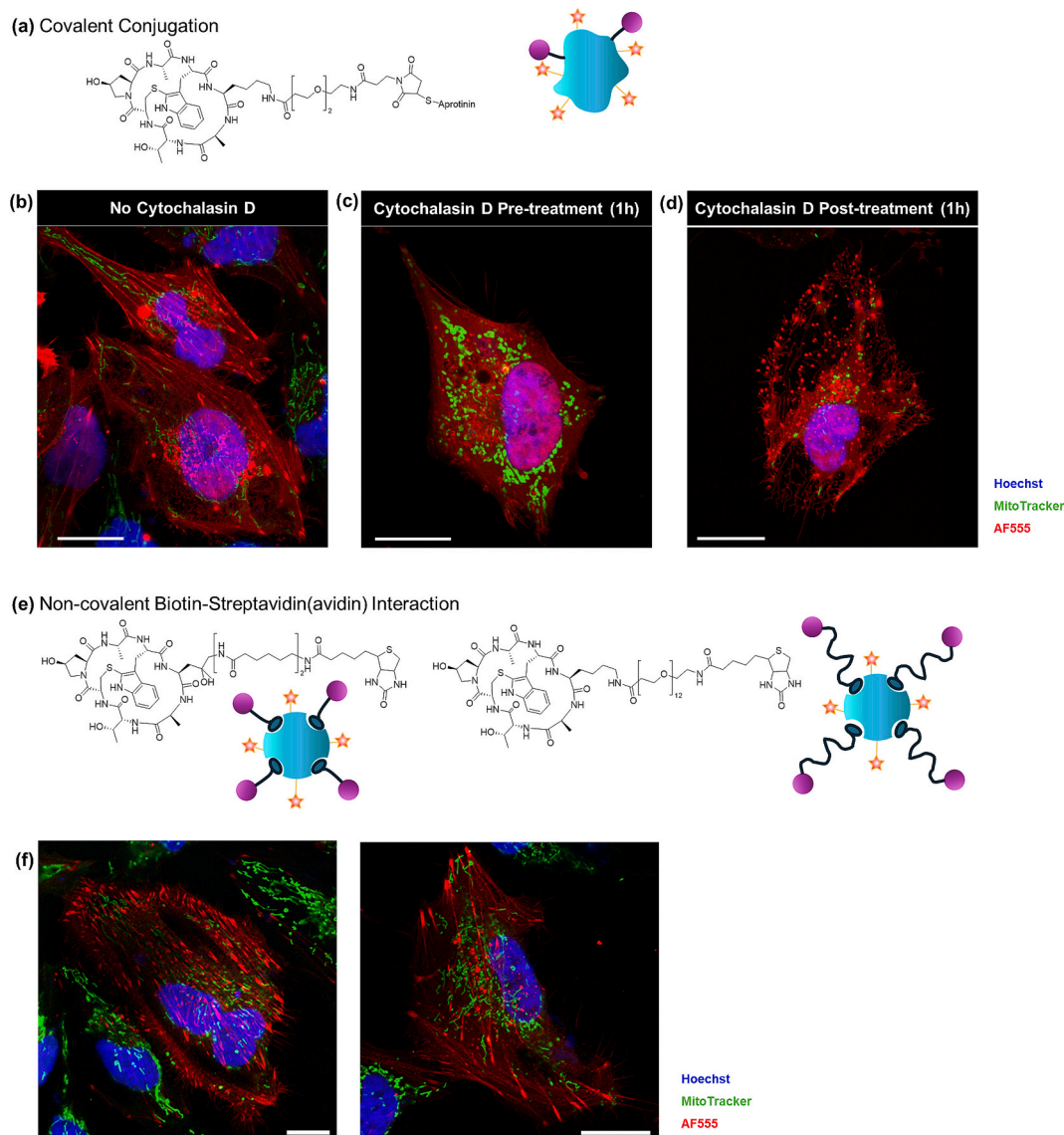


Fig. 5. Representative HeLa cells after intracellular delivery of Phalloidin conjugated Aprotinin-AF555. (a) Chemical structure and schematic illustration of Phalloidin-Aprotinin-AF555 covalent conjugates. (b) Representative confocal images of HeLa cells after intracellular delivery of Phalloidin-PEG2-Aprotinin-AF555. (100 nM, Tag ratio = 1:2) (c and d) HeLa cells treated with 10 μ M Cytochalasin D for 1 h before or after Phalloidin delivery. Scale bar: 20 μ m. (e) Chemical structures of Phalloidin-biotin conjugates with various linker length, and schematic illustration of them bound to Avidin-AF555. (f) Representative confocal images of HeLa cells after intracellular delivery of Phalloidin-PEG12-Biotin-Avidin-AF555 (100 nM, Tag ratio = 1:2). Scale bar: 20 μ m.

fluorescent, Fig. 4b). To further confirm that the vimentin was localized inside cells, confocal microscopy was used. Z-stack images clearly showed that vimentin was in the cytoplasm (Fig. 4d). Interestingly, we also noticed that the intermediate filaments mainly localized near the cell nucleus while fewer filaments were present in the cytosol (Fig. 4d, e and Supplementary Video S2), which is different from the results obtained with fixed cells (Supplementary Fig. S14). Similar observations have been made previously with a microinjected monoclonal antibody targeting the intermediate filament which rapidly condensed intermediate filaments to the peri-nuclear region [63,64]. These results underline the difference between and significance of imaging live cells over fixed cells. In contrast to the intermediate filaments in fixed cells which cannot reorganize after binding to antibodies, in live cells, intermediate filaments could be crosslinked by IgGs which are bivalent, rapidly reorganizing them to the perinuclear cap [63,64]. Moreover, it is noteworthy that, in the cytosol of live cells, specific labeling lasted for several hours offering a window for target tracking if needed. Fluorescent aggregates were observed after overnight incubation (Fig. 4c),

similar to non-specific secondary antibodies, likely due to antibody degradation and aggregation in the intracellular reducing environment.

To our surprise, unlike the anti-vimentin antibody, monoclonal antibodies against actin and β -tubulin did not show specific labeling although they share a similar structure as the vimentin antibody and they entered the cytosol at high efficiency. These two antibodies showed bright and diffuse fluorescence (Supplementary Fig. S15) similar to the secondary IgG shown in Fig. 2n. We suspected that this problem could have resulted from antibody binding to the actin/tubulin monomers or oligomers states of, or antibody perturbing the polymeric cytoskeleton structures. A literature survey revealed that depending on the binding epitopes, microtubule and actin microfilament can be disrupted by their antibodies [65–70]. Compared to intermediate filaments which form more stable bundled structures, actin and tubulin have more dynamic equilibria between the monomeric and polymeric forms. The equilibria can be shifted to the monomeric forms if antibody binding disturbs the interaction between monomers. For example, the binding of large antibodies could allosterically perturb protein structures, and/or sterically

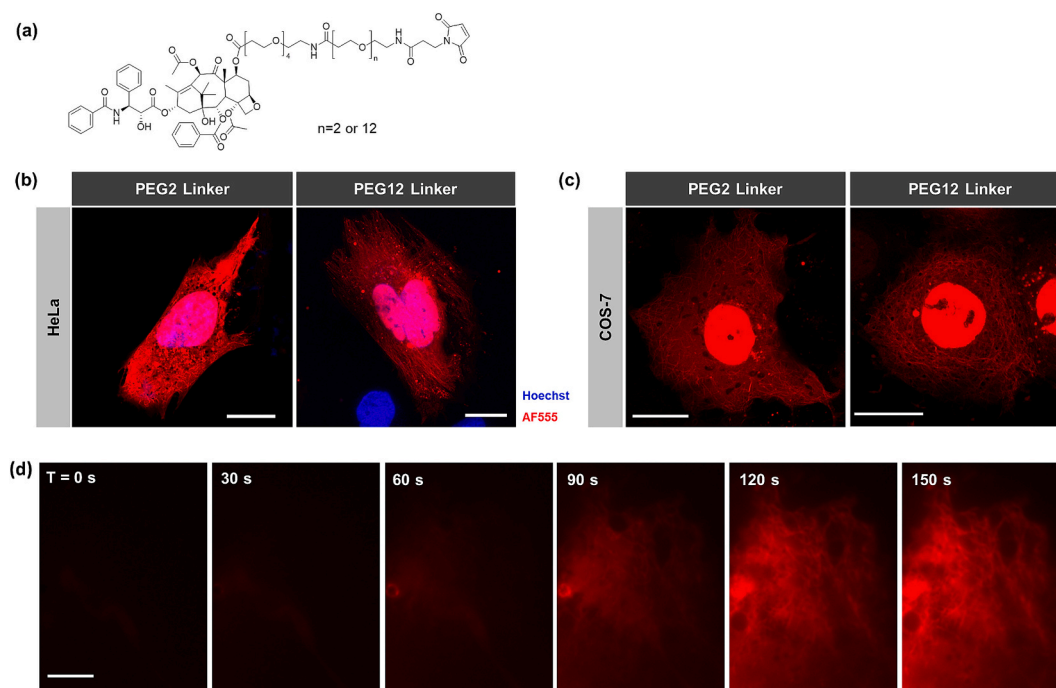


Fig. 6. Intracellular delivery of PTX-Aprotinin-AF555 conjugates. (a) Chemical structure of Paclitaxel conjugated at 7-O position with various length of pegylated maleimide linker ($n = 2$ or 12). (b) Representative confocal images of HeLa cells after intracellular delivery of PTX-Aprotinin-AF555 with PEG2, or PEG12 linker. (100 nM, Tag ratio = 1:2) Scale bar denotes 20 μm . (c) Representative confocal images of COS-7 cells after intracellular delivery of PTX-Aprotinin-AF555 with PEG2, or PEG12 linker. (100 nM, Tag ratio = 1:2) Scale bar denotes 20 μm . (d) Time-lapse imaging of COS-7 cells during delivery of PTX-PEG16-Aprotinin-AF555. (100 nM, Tag ratio = 1:2) Zoomed-out view in Supplementary Fig. S18. Fast binding kinetics of PTX-protein conjugate clearly shown by fibril structure in 60 s after cytosolic entrance. Scale bar denotes 5 μm .

interfere with binding. Although this feature is unsuited for imaging cytoskeleton in live cells, potentially it could be desirable for therapeutic applications. For the purpose of imaging actins and microtubules, we employed a new approach, using ligands that stabilize rather than disrupt the polymeric forms.

3.5. Delivery of ligand-protein conjugates for actin and microtubule

For actin, we selected phalloidin, a cyclic peptide that tightly binds to actin and prevents actin depolymerization. Phalloidin is impermeable to cell membranes, and phalloidin-AF488 conjugate cannot be delivered by the protein CB-tag because it is too small. Therefore, we used the hapten-conjugation strategy commonly used in antibody production to immobilize phalloidin to fluorescently labeled aprotinin using the cysteine-maleimide chemistry (Fig. 5a). When phalloidin-aprotinin-AF555 was delivered into cells using the CB tag, actin microfilaments became clearly visible (Fig. 5b). The labeling specificity was further proved by adding Cytochalasin D (a toxin that disrupts actin microfilaments) either before adding phalloidin-aprotinin-AF555 to cells or after the cells were already labeled with phalloidin-aprotinin-AF555. Disruption of the actin microfilament was observed regardless of the treatment sequence (Figs. 5c & d). In parallel, we also tested whether the biotin-avidin interaction can be utilized because both phalloidin-biotin and fluorescently labeled strept(avidin) are commercially available, and because the phalloidin-protein conjugates can be easily prepared by a simple incubation. When phalloidin-XX-biotin (a commercial phalloidin-biotin conjugate with a relatively short linker) was used to make the conjugate, only diffuse fluorescence inside cells was observed (Supplementary Fig. S16). When phalloidin-PEG12-biotin (a longer spacer between phalloidin and biotin) was used, actin filaments were specifically labeled similar to the covalent conjugate shown in Fig. 5f. These results show that i) strept(avidin) maintains its intact structure and binding affinity to biotin in the presence of CB-tag; ii) a long linker is

desirable to display the phalloidin moiety without creating significant steric hindrance; and iii) although similar in size, avidin has more accumulation in the nuclei over streptavidin, likely due to its cationic nature.

For microtubules, we explored the same conjugation strategy using Paclitaxel (PTX). PTX binds to the lumen of microtubules and stabilizes them, consequently preventing cell mitosis. While it has been widely prescribed to treat cancer, it can also be used for microtubule imaging [71,72]. To combine with our CB-tag technology, PTX was conjugated to Aprotinin-AF555 with PEG linkers of different lengths, PEG₂ or PEG₁₂ (Fig. 6a). When they were delivered into HeLa or COS-7 cells, both PTX-aprotinin-AF555 conjugates labeled the microtubule structure, with the longer linker showing slightly better contrast (Figs. 6b-c). It is worth mentioning that the PEG linker must be connected to PTX at the 7-O position rather than the 2'-OH position, because 2'-OH is essential for tight binding with tubulin [73] (In Supplementary Fig. S17, only diffuse fluorescence was observed with PTX functionalized at the 2'-OH position).

Using COS-7 cells which have a thin spreading morphology, we investigated the binding kinetics of PTX-aprotinin-AF555 to microtubules in live cells by time-lapse imaging with 30-s intervals (Fig. 6d, and S18). As soon as the fluorescence of PTX-aprotinin-AF555 became detectable inside cells, small fibrils of microtubule started to appear within minutes. Considering the fact that the binding site of PTX is located in the lumen of microtubules, and the relatively large size of PTX-protein, such a fast binding kinetics was somewhat surprising. Previously, using Flutax (a PTX-dye conjugate), it has also been shown that the binding site for PTX is highly accessible [74]. This accessibility has been attributed to the ability of PTX to rapidly reshape microtubules. PTX modifies the flexibility of microtubules within seconds and changes the number of protofilaments within minutes [75,76].

4. Conclusion

In summary, using the new CB-tag with an optimized protocol we demonstrated that a wide variety of proteins of interest could be transported directly into the cytosol with high efficacy, bypassing endocytosis sequestration. More importantly, delivering fluorescently labeled functional proteins into live cells not only allows direct imaging of intracellular targets of interest similar to IHC on fixed cells, but also enables the observation of cellular responses in real time. This unique feature was exemplified by the time-lapse imaging in live cells during the delivery of PTX-protein conjugates, showing rapid binding kinetics. Furthermore, we demonstrated that proteins covalently conjugated to peptides and/or small molecules or non-covalently linked through the avidin-biotin interaction could be internalized. Aided by the CB-tag, this kind of membrane permeable conjugates could find numerous applications in cell biology and drug discovery. Some examples include (i) attaching signaling peptides such as a nuclear localization signal to translocate protein cargoes into specific cellular organelles, (ii) preparing bispecific binders for induced proximity, and (iii) degrading targets by attaching E3 ligase ligands for proteolysis targeting chimera (PROTAC). It is worth highlighting that these applications are possible because CB-tag-based protein delivery does not follow the conventional endocytic pathway, instead, protein cargoes are directly transported through the plasma membrane dramatically improving the cargo bioavailability. In addition, the CB-tag approach is also simple, only requiring mixing and incubating. We envision the CB-tag to play important roles in biology research and biologics discovery.

Supplementary data to this article can be found online at <https://doi.org/10.1016/j.jconrel.2025.113651>.

CRedit authorship contribution statement

Ban-Seok Jeong: Writing – original draft, Methodology, Investigation, Formal analysis. **Hwanhee C. Kim:** Writing – original draft, Validation, Methodology, Investigation, Formal analysis. **Catherine M. Sniezek:** Methodology, Investigation. **Stephanie Berger:** Methodology, Investigation. **Justin M. Kollman:** Writing – review & editing, Supervision, Resources, Project administration, Funding acquisition, Conceptualization. **David Baker:** Writing – review & editing, Supervision, Resources, Project administration, Funding acquisition. **Joshua C. Vaughan:** Writing – review & editing, Supervision, Resources, Project administration, Funding acquisition, Conceptualization. **Xiaohu Gao:** Writing – review & editing, Supervision, Project administration, Funding acquisition, Conceptualization.

Declaration of competing interest

The authors declare that they have no known competing financial interests or personal relationships that could have appeared to influence the work reported in this paper.

Acknowledgment

This work was supported in part by the W. M. Keck Foundation (to JCV, DB, XHG, & JMK), and NIH R21CA263698 to XHG).

Data availability

Data will be made available on request.

References

- [1] A. Chan, A. Tsourkas, Intracellular protein delivery: approaches, challenges, and clinical applications, *BME Front.* 5 (2024) 0035.
- [2] L. Liu, et al., Antibodies targeting a quaternary site on SARS-CoV-2 spike glycoprotein prevent viral receptor engagement by conformational locking, *Immunity* 56 (2023) 2442–2455 e2448.
- [3] T. Oku, Y. Ando, M. Ogura, T. Tsuji, Development of splice variant-specific monoclonal antibodies against human alpha3 integrin, *Monoclon. Antib. Immunodiagn. Immunother.* 35 (2016) 12–17.
- [4] K. Singh, et al., Point mutation specific antibodies in B-cell and T-cell lymphomas and leukemias: targeting IDH2, KRAS, BRAF and other biomarkers RHOA, IRF8, MYD88, ID3, NRAS, SF3B1 and EZH2, *Diagnostics* 11 (2021).
- [5] S. Suraritdechachai, B. Lakkanasirorat, C. Uttamapinant, Molecular probes for cellular imaging of post-translational proteoforms, *RSC Chem. Biol.* 3 (2022) 201–219.
- [6] P. Chames, M. Van Regenmortel, E. Weiss, D. Baty, Therapeutic antibodies: successes, limitations and hopes for the future, *Br. J. Pharmacol.* 157 (2009) 220–233.
- [7] A.L. Nelson, Antibody fragments: hope and hype, *MAbs* 2 (2010) 77–83.
- [8] I. Jovcevska, S. Muyldermans, The therapeutic potential of Nanobodies, *BioDrugs* 34 (2020) 11–26.
- [9] F.Y. Frejd, K.-T. Kim, Affibody molecules as engineered protein drugs, *Exp. Mol. Med.* 49 (2017) e306.
- [10] F. Sha, G. Salzman, A. Gupta, S. Koide, Monobodies and other synthetic binding proteins for expanding protein science, *Protein Sci.* 26 (2017) 910–924.
- [11] M.T. Stumpp, H.K. Binz, P. Amstutz, DARPins: a new generation of protein therapeutics, *Drug Discov. Today* 13 (2008) 695–701.
- [12] A. Chevalier, et al., Massively parallel de novo protein design for targeted therapeutics, *Nature* 550 (2017) 74–79.
- [13] S. Berger, et al., Computationally designed high specificity inhibitors delineate the roles of BCL2 family proteins in cancer, *Elife* 5 (2016).
- [14] X. Lyu, et al., The global landscape of approved antibody therapies, *Antib. Ther.* 5 (2022) 233–257.
- [15] J. Lv, Q. Fan, H. Wang, Y. Cheng, Polymers for cytosolic protein delivery, *Biomaterials* 218 (2019) 119358.
- [16] E.S. Lander, et al., Initial sequencing and analysis of the human genome, *Nature* 409 (2001) 860–921.
- [17] Q. Wang, et al., Cytosolic protein delivery for intracellular antigen targeting using supercharged polypeptide delivery platform, *Nano Lett.* 21 (2021) 6022–6030.
- [18] O. Tietz, F. Cortezon-Tamarit, R. Chalk, S. Able, K.A. Vallis, Tricyclic cell-penetrating peptides for efficient delivery of functional antibodies into cancer cells, *Nat. Chem.* 14 (2022) 284–293.
- [19] J. Allen, et al., Cytosolic delivery of macromolecules in live human cells using the combined endosomal escape activities of a small molecule and cell penetrating peptide, *ACS Chem. Biol.* 14 (2019) 2641–2651.
- [20] M. Akishiba, et al., Cytosolic antibody delivery by lipid-sensitive endosomolytic peptide, *Nat. Chem.* 9 (2017) 751–761.
- [21] J.S. Andrew, et al., Sustained release of a monoclonal antibody from electrochemically prepared mesoporous silicon oxide, *Adv. Funct. Mater.* 20 (2010) 4168–4174.
- [22] D.C. Luther, et al., Delivery of drugs, proteins, and nucleic acids using inorganic nanoparticles, *Adv. Drug Deliv. Rev.* 156 (2020) 188–213.
- [23] J. Guo, et al., Rational Design of Poly(disulfide)s as a universal platform for delivery of CRISPR-Cas9 machineries toward therapeutic genome editing, *ACS Cent. Sci.* 7 (2021) 990–1000.
- [24] L. Fu, X. Hua, X. Jiang, J. Shi, Multistage systemic and cytosolic protein delivery for effective cancer treatment, *Nano Lett.* 22 (2022) 111–118.
- [25] R. Lu, et al., Reactive oxygen species-responsive branched poly(beta-amino ester) with robust efficiency for cytosolic protein delivery, *Acta Biomater.* 152 (2022) 355–366.
- [26] Y. Rui, et al., Carboxylated branched poly(beta-amino ester) nanoparticles enable robust cytosolic protein delivery and CRISPR-Cas9 gene editing, *Sci. Adv.* 5 (2019) eaay3255.
- [27] F. Hausig, et al., Correlation between protonation of tailor-made polypiperazines and endosomal escape for cytosolic protein delivery, *ACS Appl. Mater. Interfaces* 13 (2021) 35233–35247.
- [28] R. Goswami, et al., Direct cytosolic delivery of citraconylated proteins, *Pharmaceutics* 15 (2023).
- [29] M. Liang, Y. Cheng, H. Wang, A cu(+)/Thiourea dendrimer achieves excellent cytosolic protein delivery via enhanced cell uptake and endosome escape, *Chemistry* 29 (2023) e202300131.
- [30] L. Ren, J. Lv, H. Wang, Y. Cheng, A coordinative dendrimer achieves excellent efficiency in cytosolic protein and peptide delivery, *Angew. Chem. Int. Ed. Eng.* 59 (2020) 4711–4719.
- [31] S. Zhang, et al., A pH-responsive phase-transition polymer with high serum stability in cytosolic protein delivery, *Nano Lett.* 21 (2021) 7855–7861.
- [32] C. Liu, et al., A boronic acid-rich dendrimer with robust and unprecedented efficiency for cytosolic protein delivery and CRISPR-Cas9 gene editing, *Sci. Adv.* 5 (2019) eaaw8922.
- [33] X. Liu, Z. Zhao, F. Wu, Y. Chen, L. Yin, Tailoring hyperbranched poly(beta-amino ester) as a robust and universal platform for cytosolic protein delivery, *Adv. Mater.* 34 (2022) 2108116.
- [34] S. Chen, et al., Exploring the effect of Amphiphile architecture on intracellular protein delivery capacity: dimeric versus trimeric amphiphiles, *ACS Appl. Mater. Interfaces* 15 (2023) 26328–26339.
- [35] Y. Gong, S. Tian, Y. Xuan, S. Zhang, Lipid and polymer mediated CRISPR/Cas9 gene editing, *J. Mater. Chem. B* 8 (2020) 4369–4386.
- [36] M. Wang, et al., Efficient delivery of genome-editing proteins using bioreducible lipid nanoparticles, *Proc. Natl. Acad. Sci. USA* 113 (2016) 2868–2873.
- [37] M.J. Mehta, H.J. Kim, S.B. Lim, M. Naito, K. Miyata, Recent Progress in the endosomal escape mechanism and chemical structures of polycations for nucleic acid delivery, *Macromol. Biosci.* 24 (2024) e2300366.

- [38] M. Grau, E. Wagner, Strategies and mechanisms for endosomal escape of therapeutic nucleic acids, *Curr. Opin. Chem. Biol.* 81 (2024) 102506.
- [39] S. Chatterjee, E. Kon, P. Sharma, D. Peer, Endosomal escape: a bottleneck for LNP-mediated therapeutics, *Proc. Natl. Acad. Sci. USA* 121 (2024) e2307800120.
- [40] C. Qiu, et al., Advanced strategies for overcoming endosomal/lysosomal barrier in nanodrug delivery, *Research* 6 (2023) 0148.
- [41] J. Hur, A.J. Chung, Microfluidic and nanofluidic intracellular delivery, *Adv. Sci.* 8 (2021) e2004595.
- [42] V. Graceffa, Intracellular protein delivery: new insights into the therapeutic applications and emerging technologies, *Biochimie* 213 (2023) 82–99.
- [43] M.P. Stewart, R. Langer, K.F. Jensen, Intracellular delivery by membrane disruption: mechanisms, strategies, and concepts, *Chem. Rev.* 118 (2018) 7409–7531.
- [44] X. He, et al., Recent progress of rational modified nanocarriers for cytosolic protein delivery, *Pharmaceutics* 15 (2023).
- [45] R. Mout, et al., Direct cytosolic delivery of CRISPR/Cas9-ribonucleoprotein for efficient gene editing, *ACS Nano* 11 (2017) 2452–2458.
- [46] R. Mout, et al., General strategy for direct cytosolic protein delivery via protein–nanoparticle co-engineering, *ACS Nano* 11 (2017) 6416–6421.
- [47] R. Tang, Z. Jiang, M. Ray, S. Hou, V.M. Rotello, Cytosolic delivery of large proteins using nanoparticle-stabilized nanocapsules, *Nanoscale* 8 (2016) 18038–18041.
- [48] R. Tang, et al., Direct delivery of functional proteins and enzymes to the cytosol using nanoparticle-stabilized nanocapsules, *ACS Nano* 7 (2013) 6667–6673.
- [49] D.C. Luther, et al., Cytosolic protein delivery using modular biotin–streptavidin assembly of nanocomposites, *ACS Nano* 16 (2022) 7323–7330.
- [50] Y.-W. Lee, et al., Direct cytosolic delivery of proteins through coengineering of proteins and polymeric delivery vehicles, *J. Am. Chem. Soc.* 142 (2020) 4349–4355.
- [51] D.C. Luther, et al., Direct cytosolic delivery of proteins using lyophilized and reconstituted polymer–protein assemblies, *Pharm. Res.* 39 (2022) 1197–1204.
- [52] Y. Sun, X. Wu, J. Li, et al., Phase-separating peptide coacervates with programmable material properties for universal intracellular delivery of macromolecules, *Nat Commun* 15 (2024) 10094, <https://doi.org/10.1038/s41467-024-54463-z>.
- [53] A. Shebanova, et al., Cellular uptake of phase-separating peptide Coacervates, *Adv. Sci.* 11 (2024) 2402652.
- [54] Y. Sun, et al., Phase-separating peptides for direct cytosolic delivery and redox-activated release of macromolecular therapeutics, *Nat. Chem.* 14 (2022) 274–283.
- [55] T. Iwata, et al., Liquid droplet formation and facile cytosolic translocation of IgG in the presence of attenuated cationic amphiphilic lytic peptides, *Angew. Chem. Int. Ed. Eng.* 60 (2021) 19804–19812.
- [56] Z. Le, et al., Direct cytosolic delivery of proteins and CRISPR-Cas9 genome editing by Gemini Amphiphiles via non-endocytic translocation pathways, *ACS Central Sci.* 9 (2023) 1313–1326.
- [57] Y. Kawaguchi, S. Futaki, Finding ways into the cytosol: peptide-mediated approaches for delivering proteins into cells, *Curr. Opin. Chem. Biol.* 81 (2024) 102482.
- [58] R. Goswami, T. Jeon, H. Nagaraj, S. Zhai, V.M. Rotello, Accessing intracellular targets through nanocarrier-mediated cytosolic protein delivery, *Trends Pharmacol. Sci.* 41 (2020) 743–754.
- [59] W. Tai, P. Zhao, X. Gao, Cytosolic delivery of proteins by cholesterol tagging, *Sci. Adv.* 6 (2020) eabb0310.
- [60] D. Koley, A.J. Bard, Triton X-100 concentration effects on membrane permeability of a single HeLa cell by scanning electrochemical microscopy (SECM), *Proc. Natl. Acad. Sci.* 107 (2010) 16783–16787.
- [61] D.C. Luther, et al., Protein delivery: if your GFP (or other small protein) is in the cytosol, it will also be in the nucleus, *Bioconjug. Chem.* 32 (2021) 891–896.
- [62] W. Tai, X. Gao, Noncovalent tagging of siRNA with steroids for transmembrane delivery, *Biomaterials* 178 (2018) 720–727.
- [63] J.W. Klymkowsky, Intermediate filaments in 3T3 cells collapse after intracellular injection of a monoclonal anti-intermediate filament antibody, *Nature* 291 (1981) 249–251.
- [64] J.J.-C. Lin, J.R. Feramisco, Disruption of the in vivo distribution of the intermediate filaments in fibroblasts through the microinjection of a specific monoclonal antibody, *Cell* 24 (1981) 185–193.
- [65] D. Dalkara, G. Zuber, J.P. Behr, Intracytoplasmic delivery of anionic proteins, *Mol. Ther.* 9 (2004) 964–969.
- [66] V. Postupalenko, et al., Protein delivery system containing a nickel-immobilized polymer for Multimerization of affinity-purified his-tagged proteins enhances cytosolic transfer, *Angew. Chem. Int. Ed. Eng.* 54 (2015) 10583–10586.
- [67] O. Skalli, F. Gabbiani, G. Gabbiani, Action of general and α -smooth muscle-specific actin antibody microinjection on stress fibers of cultured smooth muscle cells, *Exp. Cell Res.* 187 (1990) 119–125.
- [68] A. Fuchtbauer, M. Herrmann, E.M. Mandelkow, B.M. Jockusch, Disruption of microtubules in living cells and cell models by high affinity antibodies to β -tubulin, *EMBO J.* 4 (1985) 2807–2814.
- [69] B.M. Jockusch, C.J. Temm-Grove, Microinjection of antibodies in the analysis of cellular architecture and motility, *Methods Cell Biol.* 37 (1993) 343–359.
- [70] J. Wehland, H.C. Schröder, K. Weber, Contribution of microtubules to cellular physiology: microinjection of well-characterized monoclonal antibodies into cultured cells, *Ann. N. Y. Acad. Sci.* 466 (1986) 609–621.
- [71] I. Barasoain, J.F. Díaz, J.M. Andreu, in: L. Wilson, J.J. Correia (Eds.), *Methods in Cell Biology* vol. 95, Academic Press, 2010, pp. 353–372.
- [72] J.A. Evangelio, et al., Fluorescent taxoids as probes of the microtubule cytoskeleton, *Cell Motil.* 39 (1998) 73–90.
- [73] S. Sharma, et al., Dissecting paclitaxel-microtubule association: quantitative assessment of the 2'-OH group, *Biochemistry* 52 (2013) 2328–2336.
- [74] J.F. Diaz, I. Barasoain, J.M. Andreu, Fast kinetics of Taxol binding to microtubules. Effects of solution variables and microtubule-associated proteins, *J. Biol. Chem.* 278 (2003) 8407–8419.
- [75] J.F. Diaz, J.M. Valpuesta, P. Chacón, G. Diakun, J.M. Andreu, Changes in microtubule Protofilament number induced by Taxol binding to an easily accessible site: internal microtubule dynamics, *J. Biol. Chem.* 273 (1998) 33803–33810.
- [76] R.B. Dye, S.P. Fink, R.C. Williams, Taxol-induced flexibility of microtubules and its reversal by MAP-2 and tau, *J. Biol. Chem.* 268 (1993) 6847–6850.